Research Article

Nadja Felde*, Luisa Coriand, Sven Schröder, Angela Duparré and Andreas Tünnermann

Defined wetting properties of optical surfaces

DOI 10.1515/aot-2017-0028
Received April 10, 2017; accepted May 8, 2017; previously published online June 9, 2017

Abstract: Optical surfaces equipped with specific functional properties have attracted increasing importance over the last decades. In the light of cost reduction, hydrophobic self-cleaning behavior is aspired. On the other side, hydrophilic properties are interesting due to their anti-fog effect. It has become well known that such wetting states are significantly affected by the surface morphology. For optical surfaces, however, this fact poses a problem, as surface roughness can induce light scattering. The generation of optical surfaces with specific wetting properties, hence, requires a profound understanding of the relation between the wetting and the structural surface properties. Thus, our work concentrates on a reliable acquisition of roughness data over a wide spatial frequency range as well as on the comprehensive description of the wetting states, which is needed for the establishment of such correlations. We will present our advanced wetting analysis for nanorough optical surfaces, extended by a vibration-based procedure, which is mainly for understanding and tailoring the wetting behavior of various solid-liquid systems in research and industry. Utilizing the relationships between surface roughness and wetting, it will be demonstrated how different wetting states for hydrophobicity and hydrophilicity can be realized on optical surfaces with minimized scatter losses.

***Corresponding author: Nadja Felde,** Fraunhofer Institute for Applied Optics and Precision Engineering, Albert-Einstein-Strasse 7, 07745 Jena, Germany; and Friedrich Schiller University, Institute of Applied Physics, Abbe Center of Photonics, Albert-Einstein-Str. 6, 07745 Jena, Germany, e-mail: nadja.felde@iof.fraunhofer.de
Luisa Coriand, Sven Schröder and Angela Duparré: Fraunhofer Institute for Applied Optics and Precision Engineering, Albert-Einstein-Strasse 7, 07745 Jena, Germany
Andreas Tünnermann: Fraunhofer Institute for Applied Optics and Precision Engineering, Albert-Einstein-Strasse 7, 07745 Jena, Germany; and Friedrich Schiller University, Institute of Applied Physics, Abbe Center of Photonics, Albert-Einstein-Str. 6, 07745 Jena, Germany

www.degruyter.com/aot

Keywords: contact angle; light scattering; surface roughness; thin films; wetting properties.

OCIS codes: 120.6660 surface measurements, roughness; 160.4236 nanomaterials; 310.6860 thin films, optical properties; 310.6870 thin films, other properties.

1 Introduction

The wetting behavior of surfaces is of enormous importance for many applications, which is evident by the increased research on, e.g. hydrophobic and oleophobic surfaces [1–3], anti-fog coatings [4, 5], as well as anti-icing properties [6–8]. In particular, optical components with extreme wetting behavior have attracted rapidly growing interest over the last decades. Glass surfaces, e.g. with superhydrophobic – severely water repelling – properties are in great focus, as the related effect of self-cleaning significantly decreases their maintenance costs. Similar raising interest has also been expressed for oleophobic – oil-repelling – optical surfaces, especially in the industry sector for optical underwater sensors. However, each application demands specially tailored wetting properties. The precise adjustment of the desired wetting behavior of optical surfaces, therefore, presupposes a profound understanding of the wetting processes in relation to their structural and optical surface properties.

In general, surface wetting is described by three involved phases: the solid, the liquid, and the surrounding fluid. The main parameter is the angle formed between the liquid drop and the solid surface, the so-called contact angle (CA) [9]. For a given system, there are two key mechanisms to tailor the CA: first, the chemical aspect with the change in the surface free energy of the solid; second, the morphological aspect, which requires an increase in the surface roughness [10–12]. For the formation of extreme wetting properties (e.g. superhydrophobicity), modification of surface chemistry must always be combined with surface roughness enhancement. Note that even a material with the lowest surface free energy, defined by regularly aligned closest-hexagonal-packed CF_3 groups provides water CAs of only 120° if the surface is smooth [13]. The enhancement of the predominant wetting state by surface roughness bases theoretically on

well-established models [14, 15]. In practice, this assumes knowledge about the wetting relevant surface roughness and an applicable technology to generate this specific surface structure.

However, in view of optical surfaces, roughness structures, although needed for the extreme wetting behavior, can also become a critical point for the optical quality as they increase light scattering [16, 17]. This contradiction in the requirements on using rough structures to generate functionality and low roughness to maintain low scattering can only be solved by tailoring the roughness spectrum in the relevant spatial frequency region. A nowaday-proven strategy is to shift the roughness structures to the nanoscale. A large number of papers have been published dealing with nanorough transparent coatings, especially with superhydrophobic properties [18–20]. In spite of enormous research, variations in the CA tailored to the specific application are not provided.

Our work, therefore, addresses the specific adjustment of the wetting behavior of optical surfaces with minimized light scattering through adjustable surface roughness. This implies, in particular, a throughout characterization of the structural surface properties within the application-relevant spatial frequency range using power spectral density functions as well as tailored wetting characterization methods orientated toward the predominant wetting state. We will present our practice-oriented methodology for wetting analysis extended by an advanced vibration-based procedure, which allows a more precise connection of roughness and wetting data to adjust and predict the wetting properties for optical surfaces. Utilizing these methods enables the generation of surfaces with defined wetting properties and minimized light scattering at the same time. The methodology will be verified utilizing model coatings on glass surfaces with adjustable nanoroughness.

2 Basics and experimental

2.1 Wetting

The wetting behavior of real solid surfaces is generally dominated by two factors: the surface free energy and the morphology of the surface. For ideal surfaces, the CA depends only on the surface tensions at the solid-air (γ_{sa}), solid-liquid (γ_{sl}), and liquid-air (γ_{la}) interface [21]:

$$\cos\theta_Y = \frac{\gamma_{sa} - \gamma_{sl}}{\gamma_{la}} \tag{1}$$

Utilizing this theoretical fundamental, wetting can be classified into two general states: in the case of hydrophilicity, water-attracting behavior, the so-called Young-CA θ_Y is defined lower than 90°. For hydrophobicity, water-repelling behavior, holds $\theta_Y > 90°$. However, the Young-CA, describes wetting on a non-reactive, homogeneous, and smooth surface. Nevertheless, surfaces of technical interest are defined by surface roughness, which leads, e.g. for a liquid droplet thermodynamically to multiple energy minima in contrast to ideal surfaces with one global minimum, as discussed in Ref. [9] and outlined in Section 3.3. This range of metastable states is defined by the CA hysteresis and is limited by the highest, specified as the advancing CA (ACA), and the lowest observable, the so-called receding CA (RCA). The metastable states are separated by discrete energy barriers, which need to be overcome to reach the most stable state of the wetting system.

Theoretically, the relation between surface roughness and the CA is described by two classical models of Wenzel or Cassie-Baxter [14, 15]. Based, e.g. on the assumption that the liquid is completely covering the solid surface, the Wenzel regime is applied [14]:

$$\cos\theta_W = r\cos\theta_Y, \tag{2}$$

where the Wenzel CA θ_w describes the most stable CA (MSCA) and r the roughness ratio, defined as the ratio between the actual and projected surface area. The main factor, controlling the wetting is, hence, the surface roughness.

2.2 Roughness measurement and analysis

The assessment of roughness information within a wide range of surface structures was based on the combination of different roughness measurement techniques. In this paper, roughness analysis in the high spatial frequency range ($f > 1\ \mu m^{-1}$) was performed using a Dimension Icon Atomic Force Microscope (AFM) from Bruker (Santa Barbara, CA, USA). The AFM was operated in tapping mode utilizing single crystalline Si probes with a nominal tip radius of 7 nm. The roughness data were complemented by white light interferometry (WLI) analysis in the mid-spatial frequency range ($0.001\ \mu m^{-1} < f < 1\ \mu m^{-1}$) using the NewView7300 instrument from ZygoLOT Europe GmbH (Dramstadt, Germany). The data was analyzed utilizing power spectral density (PSD) functions. PSDs represent the power of different roughness components as a function of the spatial frequencies f_x, f_y within the measurement area L^2 [22]:

$$PSD(f_x, f_y) = \lim_{L\to\infty} \frac{1}{L^2} |FT[z(x,y)]|^2 . \tag{3}$$

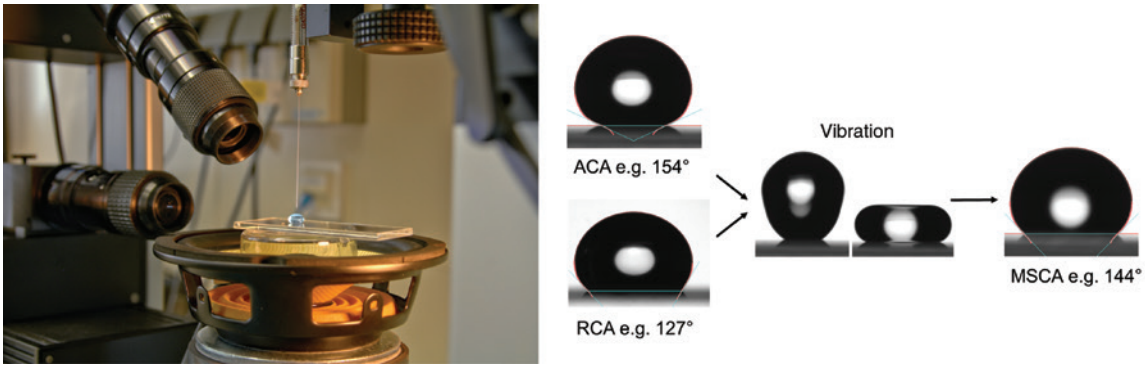

Figure 1: Vibration-based CA measurement setup (left); illustrated measurement procedure (right).

In the case of isotropic surfaces, such as stochastic nanostructures, azimuthal averaging in polar coordinates can be performed to calculate the 2D-isotropic PSD(f). Using this function, the bandwidth-limited rms-roughness, as presented in the following equation, was calculated [22]:

$$\mathrm{rms} = \sqrt{2\pi \int_{f_{min}}^{f_{max}} f\,\mathrm{PSD}(f)\,df}. \tag{4}$$

2.3 Wetting measurement and analysis

For the analysis of the wetting properties, the CA measurement system OCA20 from DataPhysics GmbH (Filderstadt, Germany) was used. As introduced in Section 2.1, real solid surfaces are characterized by a wide range of metastable CAs. To cover this spectrum, the observation of the ACA and RCA is indispensable. The measurement procedure is based on the deposition of a drop on the solid surface with the needle-in method. ACA and RCA are detected by varying the drop volume and observation of advancing and receding of the drop at the three-phase contact line (for a detailed description, see Ref. [23]). Furthermore, considering hydrophobic surfaces, knowledge of the slide-off and roll-off behavior of the liquid drops is a main characterization factor. For this propose, the minimum tilt angle α of the surface, which causes a drop, placed on the surface, to start sliding or rolling off, was determined [24]. In the case of no presence of sliding or rolling behavior, which holds true, in particular, for high CA hysteresis, the bounce-off angle was determined. This angle is tantamount to the angle of the tilted surfaces from which a drop can jump-off when falling from a certain height [24].

However, thermodynamically most meaningful is the CA that occurs when the system reaches its global minimum. In contrast to ACA and RCA, this MSCA is closely related to the surface free energy of the solid [23, 25]. Thus, we established an advanced methodology to determine the MSCA using the mechanical vibration of sessile drops, starting from the metastable ACA and RCA states. The specific setup is illustrated in Figure 1 (left).

The system consists of a loudspeaker with an amplifier, which we have integrated in the CA measurement system OCA20. An oscilloscope was used to monitor the voltage of the input vibration. In this setup, the investigated surfaces were placed horizontally in the center of the loudspeaker. The applied water drops (volume: 50 µl) were then vibrated with a frequency-modulated sine wave signal, while the vibration amplitude was quantified from the side-view with the camera system. The measurements started at the ACA or RCA state, whereby the vertical vibration amplitude was gradually increased from 0 mm to 0.2 mm with the aim to overcome the individual energy barriers between the metastable states of the CA (see Figure 1, right). In addition to the side-view observation of the drops, top-view images were made to ensure that the drops are axisymmetric.

However, the presented methods are not applicable to hydrophilic surfaces due to the vanishing RCA and, consequently, the reduced contrast between the drop, surface, and environment. Therefore, for hydrophilic surfaces, the CA was characterized by determination of the apparent CA as a function of the wetting time t [24].

2.4 Light-scattering measurements

To verify the aspired minimized light scattering of the optical surfaces, measurements were performed with the table top light scatterometer Albatross-TT developed at Fraunhofer IOF (Jena, Germany) [26]. The wavelength was chosen to be 640 nm as it is relevant for visible light

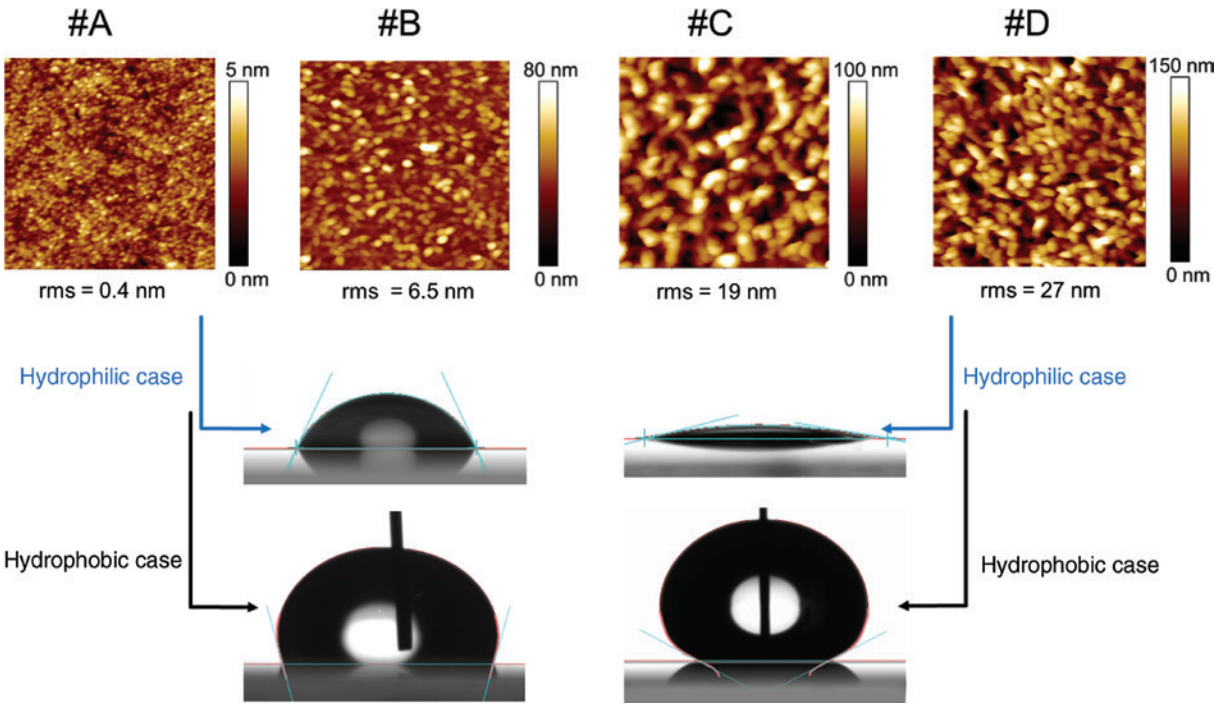

Figure 2: AFM images (scan area: 1×1 µm²) for samples #A to #D and corresponding wetting behavior for samples #A and #D in the case of hydrophilicity (CA for t = 2.5 s) and hydrophobicity – after application of a thin hydrophobic top layer (ACA).

applications. In the measurement regime, the angle resolved scattering (ARS) [16, 27], defined as the scattered power into a certain solid angle normalized to that solid angle and to the incident light power, was recorded within the transmission hemisphere at an angle of incidence of 0°. By integration of the ARS data, the total scatter (TS) was calculated as well [28]:

$$TS = 2\pi \int_{2^\circ}^{85^\circ} ARS(\theta_s) \sin\theta_s d\theta_s . \quad (5)$$

2.5 Samples

To demonstrate the adjustment of defined wetting states by surface roughness, nanorough model coatings on glass were generated. Sol-gel processes in combination with dip coating were chosen, as both processes allow a quite easy and flexible adjustment of the deposition parameters [29]. The coatings were based on Al_2O_3 films deposited on borosilicate glass substrates. The roughness of the thin films was adjustable through changing the dip-coating process parameters and a further thermal treatment of the samples. Applying an additional thin perfluorpolyether top layer Duralon UltraTec from Cotec GmbH (Karlstein a. Main, Germany) by dip-coating turned the intrinsic hydrophilic Al_2O_3 material into a hydrophobic surface.

3 Results and discussion

3.1 Graded surface roughness and light scattering

In Figure 2, AFM topographies of the Al_2O_3 coatings on glass substrates are depicted together with the corresponding rms-roughness values. As intended, a growth of the nanostructures from sample #A to #D is particularly present. The increased surface nanoroughness was realized by well-defined manufacturing parameters. All samples, except the smoothest sample #A, exhibit the flower-like surface characteristic, which is typical for the Al_2O_3 coatings [30]. However, the rough structure is only dominant in the high spatial frequency range, as illustrated in Figure 3, presenting the combined PSD functions of AFM and WLI measurements. Within the PSD diagram, the most significant part of the thin film roughness evolution is located at spatial frequencies ranging from 1 µm^{-1} to 1000 µm^{-1}, whereas almost identical PSD functions at frequencies lower than f < 0.07 µm^{-1} indicate an almost perfect replication of the substrate roughness.

Using Eq. (4), the rms-roughness was calculated in the mid-spatial frequency and in the high-spatial frequency ranges. The mid-spatial frequency range is retrieved from

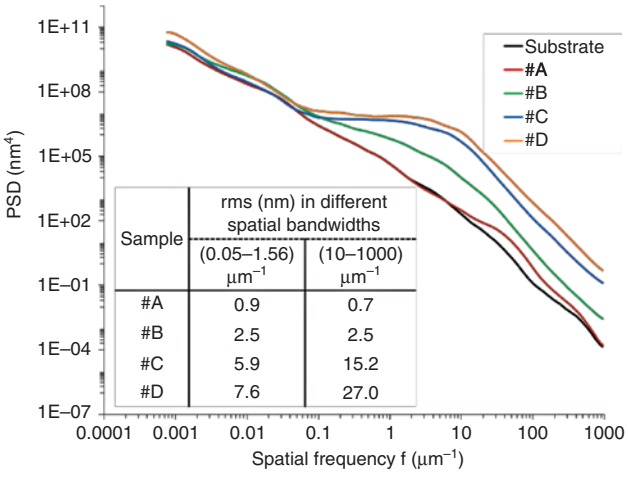

Figure 3: PSD functions for samples #A to #D in comparison to the PSD function of the glass substrate and rms-roughness values in the high- and mid-spatial frequency range.

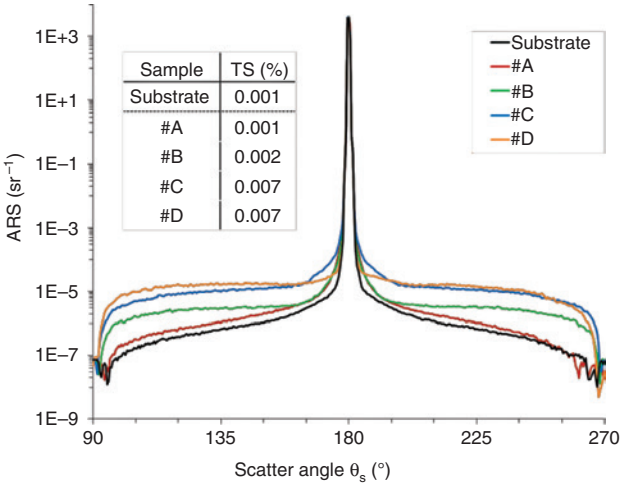

Figure 4: ARS measurement for samples #A to #D in comparison to the ARS measurement of the glass substrate and calculated TS values.

the correlation between the ARS and the roughness spectrum PSD [16, 17]:

$$\mathrm{ARS}(\theta_s) = \mathrm{QPSD}(f), \tag{6}$$

where the optical factor Q contains information about the illumination and observation conditions as well as material properties. Within this equation, the spatial frequencies and the scattering angles θ_s are related through the grating equation [16]:

$$f = \frac{\sin\theta_s}{\lambda}. \tag{7}$$

For an illumination wavelength of 640 nm and scattering angles between 2° and 85°, the relevant spatial frequencies for normal incidence, consequently, range between 0.05 µm^{-1} and 1.56 µm^{-1}. However, the high spatial frequency range between 10 µm^{-1} and 1000 µm^{-1} has been shown in previous works as to be wetting relevant for nanorough optical coatings [31]. The results are presented in Figure 3 as well. The data confirm the statement that the most significant part of the increased thin film roughness is located in the high, i.e. wetting relevant, spatial frequency part. Consequently, light scattering is not significantly affected by that increased nanoroughness. Selected ARS data are shown in Figure 4. The calculated TS values in accordance with Eq. (5) underline these results: even the roughest sample #D reveals only slightly higher TS values compared to the glass substrate surface.

This precise spatial adjustment of the surface roughness, hence, facilitates both the realization of the roughness needed to achieve the desired wetting behavior, as will be illustrated in the following section, and a reduction of roughness-induced light scattering by shifting the roughness components into the high spatial frequency range.

3.2 Hydrophilic and hydrophobic surface properties

As revealed in Figure 2, the defined wetting properties of optical surfaces can be dominated by the surface nanoroughness. Increasing the roughness corresponds to increased effects of the predominant wetting states, as introduced in the theoretical models in Section 2.1. Regarding the pure Al_2O_3 coatings with high surface free energy ($\theta_Y < 90°$), surface roughness results in decreasing CAs from samples #A to #D. Sample #D, defined by a high aspect ratio of the structures, shows CAs even lower than 5° within only a few seconds of wetting. This behavior can be correlated to superhydrophilicity. Table 1 summarizes the achieved wetting properties. The results demonstrate

Table 1: Wetting behavior of samples #A to #D.

Sample	#A	#B	#C	#D
CA (t = 0 s)	65°	37°	18°	14°
CA (2.5 s < t < 10 s)	64°	36°	6°	4°
ACA/RCA	111°/96°	120°/92°	154°/83°	154°/145°
α	28°	28°	59°	3°

CA as a function of the wetting time for hydrophilic coatings; ACA, RCA, and roll-off angle for coatings after applying an additional thin hydrophobic top layer.

that the CA is adjustable between 64° and complete wetting with CAs < 5°.

However, in the case of surfaces with low surface free energy, defined by $\theta_Y > 90°$, the increased nanoroughness results in increased CAs, ACA and RCA, respectively (see Figure 2). For sample, #D the CA hysteresis, calculated by the subtraction of ACA and RCA, is decreased to as low as 10° (cf. Table 1). This means that increased roughness reduces the range of metastable CAs in comparison to moderate rough surfaces. This behavior can be explained by the transition from the Wenzel wetting state, where the drop completely covers the solid surface (samples #A to #C), to the Cassie-Baxter state (sample #D), which is characterized by air trapped between the drop and the solid surface [14, 15, 23]. Utilizing these nanorough coatings on optical components, the ACA can be adjusted between 111° and 154°. Furthermore, the roll- and slide-off behavior is controlled by the surface structures. Whereas on samples #A to #C the drops tend to stick on the surface, sample #D reveals very low roll-off angles of 3°, confirming the reduced interface between the drop and the solid surface due to the heterogeneous wetting state. Hence, sample #D can be classified as superhydrophobic in accordance to Ref. [32]. However, some practical applications of optical surfaces do not require such extreme wetting properties. In cases where kinetic energy plays an additional role, exemplarily in case of moving optics, roughness structures like those of sample #C are sufficient to achieve self-cleaning properties [33]. Here, low bounce-off angles of 20° lead to a removal of the contaminations by minimized adhesion forces of the particles to the surface compared to the drop.

3.3 Most stable contact angle

In the previous section, it has been demonstrated that the adjustment of hydrophilicity or hydrophobicity for optical applications is based on adjustable surface roughness in the nanorange. Using theoretical models or empirical relationships between the contact angles and the roughness spectrum, as exemplarily described in Refs. [32, 34, 35], allows a precise prediction and generation of surfaces with defined wetting properties. This establishment of relations between the CA and the surface roughness, however, necessitates a reliable characterization of the wetting properties. In general, ACA and RCA are an appropriate approach, as they cover the whole spectrum of observable CAs. However, a more precise characterization bases on the determination of the MSCA, as it is defined by the global minimum in the Gibbs energy curve, depicted in Figure 5 (left). Utilizing Eq. (2) in combination with the roughness spectrum of the surface, the MSCA can be related to the Young-CA and provides insight into the surface free energy [9].

The measurement of this CA is extremely challenging because the energy barrier between the metastable states has to be overcome. In the literature, several approaches were suggested to calculate or measure the MSCA (see, e.g. Refs. [36] and [37] and overview in Refs. [38] and [39]). The direct estimation of the MSCA bases, in general, on supplying energy to the wetting system in the form of vibration. Here, different conditions are used in reaching the MSCA. In Ref. [37], exemplarily, it is assumed that the drop is axisymmetric if the global minimum is reached, observing the drops from the top-view. For this investigation, the

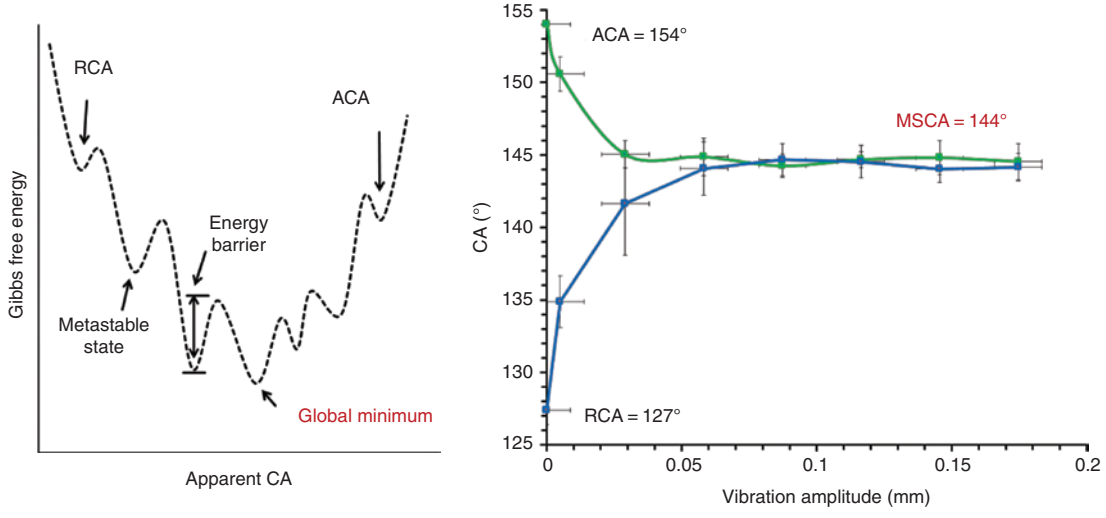

Figure 5: Gibbs free energy curve (left); CA as a function of vibration amplitude for a nanorough Al_2O_3 sample with hydrophobic top layer (right).

authors used rough glass samples with roughness values in the micrometer range. Prevalent for these investigations are, however, polymer samples also with roughness values up to microns (see, e.g. Ref. [40]).

Unlike this, we established a procedure for direct measurement of the MSCA on nanorough surfaces using vibrations. The measurements are based on the ACA/RCA method with investigation of the CA from the side-view. The results of this experimental procedure are presented on a nonorough Al_2O_3 sample with an additional hydrophobic top layer. As seen in Figure 5 (right), starting from the ACA (CA = 154°), the increased vertical vibration amplitude from 0 mm to 0.2 mm allows the drop to overcome the energy barriers between separate metastable states. In accordance to the Gibbs energy curve (see Figure 5, left), the CA decreases starting from the ACA state. In case of RCA (CA = 127°), the CA increases when applying energy in the form of vibrations. The MSCA was finally defined as the CA that remained unchanged after further increase in the vibration amplitude (CA = 144°). The experiments showed that a vibration frequency of 30 Hz is optimal for nanorough optical coatings. In this case, a vibration time of 90 s is sufficient to reach a further metastable state. It was assumed that higher frequencies will have a positive impact on the transition between the individual metastable states. However, we observed that the standard deviation of the values was significantly increased at higher frequencies. This was caused by the irregular drop shape, which was monitored by the top-view camera.

However, Marmur et al. reported in Ref. [23] that the CA measured after vibration does not necessarily correspond to the global minimum of the Gibbs energy curve. Nevertheless, the obtained CA is more precise than the ACA and RCA values and, hence, provides a more reliable characterization of the wetting system.

4 Summary

The presented study addressed the tailored hydrophobic and hydrophilic wetting properties on optical surfaces. A methodology of precise characterization of roughness and wetting was demonstrated, which constitutes the basis for the establishment of reliable correlations between these surface properties. It was shown that wide-scale roughness analysis using power spectral density functions is essential for a harmonized adjustment of the wetting and optical properties. For a complete description of hydrophobic surfaces, the determination of the advancing and receding contact angles in combination with the roll-off and bounce-off behavior was presented. Additionally, an advanced vibration-based method for the estimation of the most stable contact angle was introduced. It was shown that the roughness-induced energy barriers between the metastable contact angles on nanorough optical surfaces can be overcome by vertical vibration with a frequency of 30 Hz and an amplitude of about 0.1 mm. In combination with the measured surface roughness spectrum, this parameter can even be correlated to the intrinsic material properties of the surface. Altogether, the presented methodology provides a reliable basis for analyzing, understanding, and finally tailoring the wetting behavior of optical components. Nanorough Al_2O_3 sol-gel model coatings were used to validate the procedure and to demonstrate the ability to precisely adjust the hydrophilicity and hydrophobicity of surfaces while maintaining low scatter losses. As to the hydrophobic case, advancing contact angles between 111° and 154°, i.e. even superhydrophobic behavior, could be realized.

Acknowledgments: We gratefully acknowledge the contributions of Daniel Nebule Gurevich (Technion/Israel) and Anne-Sophie-Munser (Fraunhofer IOF) to these investigations.

References

[1] F. Horowitz, L. E. V. S. Brandão, K. C. Camargo, A. F. Michels and N. M. Balzaretti, J. Nanophotonics 7, 73596 (2013).
[2] P. Ragesh, V. Anand Ganesh, S. V. Nair and A. S. Nair, J. Mater. Chem. 2, 14773 (2014).
[3] T. C. Rangel, A. F. Michels, F. Horowitz and D. E. Weibel, Langmuir 31, 3465 (2015).
[4] P. Patel, C. K. Choi and D. D. Meng, J. Assoc. Lab. Autom. 15, 114 (2010).
[5] J. Zhao, L. Ma, W. Millians, T. Wu and W. Ming, ACS Appl. Mater. Interfaces 8, 9737 (2016).
[6] L. Cao, A. K. Jones, V. K. Sikka, J. Wu and D. Gao, Langmuir 25, 12444 (2009).
[7] L. Mazzola, Surf. Eng. 32, 733 (2016).
[8] L. Mazzola, G. Bruno, B. Galasso, V. Quaranta, F. Albano, et al., J. Aeronaut. Aerosp. 6, 1 (2017).
[9] A. Marmur, Annu. Rev. Mater. Res. 39, 473 (2009).
[10] D. Quéré, Phys. A Stat. Mech. its Appl. 313, 32 (2002).
[11] A. Marmur, Langmuir 19, 8343 (2003).
[12] M. Ramiasa-MacGregor, A. Mierczynska, R. Sedev and K. Vasilev, Nanoscale 8, 4635 (2016).
[13] T. Nishino, M. Meguro, K. Nakamae, M. Matsushita and Y. Ueda, Langmuir 15, 4321 (1999).
[14] R. N. Wenzel, Ind. Eng. Chem. 28, 988 (1936).
[15] A. B. D. Cassie, S. Baxter, Trans. Faraday Soc. 40, 546 (1944).
[16] J. C. Stover, Optical Scattering: Measurement and Analysis, Third edition, (SPIE Press, Bellingham, Wash, 2012).
[17] S. Schröder, M. Trost, M. Garrick, A. Duparré, X. Cheng, et al., Thin Solid Films 592, 248 (2015).

[18] M. Flemming and A. Duparré, Appl. Opt. 45, 1397 (2006).
[19] Y. Xiu, F. Xiao, D. W. Hess and C. P. Wong, Thin Solid Films 517, 1610 (2009).
[20] C. Su, J. Li, H. Geng, Q. Wang and Q. Chen, Appl. Surf. Sci. 253, 2633 (2006).
[21] T. Young, Philos. Trans. R. Soc. London 95, 65 (1805).
[22] A. Duparré, J. Ferre-Borrull, S. Gliech, G. Notni, J. Steinert, et al., Appl. Opt. 41, 154 (2002).
[23] A. Marmur, Soft Matter 2, 12 (2006).
[24] L. Coriand, M. Mitterhuber, A. Duparré and A. Tünnermann, Appl. Opt. 50, C257 (2011).
[25] A. Marmur, Colloids Surf. A Physicochem. Eng. Asp. 116, 55 (1996).
[26] A. von Finck, T. Herffurth, S. Schröder, A. Duparré and S. Sinzinger, Appl. Opt. 53, A259 (2014).
[27] S. Schröder, A. von Finck and A. Duparré, Adv. Opt. Technol. 4, 361 (2015).
[28] ISO 13696:2002 – Optics and optical instruments – test methods for radiation scattered by optical components (2002).
[29] C. J. Brinker, G. C. Frye, A. J. Hurd and C. S. Ashley, Thin Solid Films 201, 97 (1991).
[30] T. Minami, N. Katata and K. Tadanaga, SPIE 3136, 168 (1997).
[31] M. Flemming, L. Coriand and A. Duparré, J. Adhes. Sci. Technol. 23, 381 (2009).
[32] A. Duparré and L. Coriand, in: Adv. Contact Angle, Wettability Adhes, Ed. by K. L. Mittal (John Wiley & Sons, Inc., Hoboken, NJ, USA, 2013) pp. 197–201.
[33] D. Bartolo, F. Bouamrirene, E. Verneuil, A. Buguin, P. Silberzan, et al., Europhys. Lett. 74, 299 (2006).
[34] H. Awada, B. Grignard, C. Jérôme, A. Vaillant, J. De Coninck, et al., Langmuir 26, 17798 (2010).
[35] F. Bottiglione and G. Carbone, J. Phys. Condens. Matter 27, 015009 (2015).
[36] J. A. White, M. J. Santos, M. A. Rodríguez-Valverde and S. Velasco, Langmuir 31, 5326 (2015).
[37] T. S. Meiron, A. Marmur and I. S. Saguy, J. Colloid Interface Sci. 274, 637 (2004).
[38] E. Chibowski, Adv. Colloid Interface Sci. 133, 51 (2007).
[39] F. J. Montes Ruiz-Cabello, M. A. Rodríguez-Valverde and M. A. Cabrerizo-Vílchez, Adv. Colloid Interface Sci. 206, 320 (2014).
[40] M. A. Rodríguez-Valverde, F. J. Montes Ruiz-Cabello and M. A. Cabrerizo-Vílchez, Soft Matter 7, 53 (2011).